

University of Arkansas, Fayetteville

ScholarWorks@UARK

Civil Engineering Undergraduate Honors Theses

Civil Engineering

5-2016

Validation of an Internal Camera Based Volume Determination System for Triaxial Testing

Leah D. Miramontes

University of Arkansas, Fayetteville

Follow this and additional works at: <https://scholarworks.uark.edu/cveguht>



Part of the [Civil Engineering Commons](#), [Geotechnical Engineering Commons](#), and the [Soil Science Commons](#)

Citation

Miramontes, L. D. (2016). Validation of an Internal Camera Based Volume Determination System for Triaxial Testing. *Civil Engineering Undergraduate Honors Theses* Retrieved from <https://scholarworks.uark.edu/cveguht/33>

This Thesis is brought to you for free and open access by the Civil Engineering at ScholarWorks@UARK. It has been accepted for inclusion in Civil Engineering Undergraduate Honors Theses by an authorized administrator of ScholarWorks@UARK. For more information, please contact scholar@uark.edu, uarepos@uark.edu.

Validation of an Internal Camera Based
Volume Determination System for Triaxial Testing

A thesis submitted in partial fulfillment
of the requirements for the degree of
Bachelor of Science in Civil Engineering

by

Leah D. Miramontes

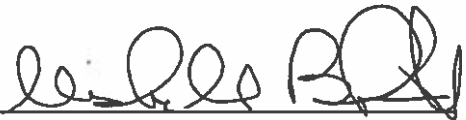
May 2016
University of Arkansas



Dr. Richard A. Coffman
Thesis Director



Dr. Kevin D. Hall
Committee Member



Dr. Michelle Bernhardt
Committee Member

Table of Contents

Abstract	3
Introduction and Background	4
Validation of the Internal Photogrammetry Technique.....	6
Calibration of Board Cameras.....	7
Derivation of Camera Locations and Orientations within the Triaxial Cell	7
Determination of Photograph-Capturing Intervals.....	8
Capture of Photographs of Acrylic Specimen.....	9
Photogrammetric Reconstruction of a Specimen.....	10
Determination of a Specimen Volume	11
Evaluation of Accuracy of Technique.....	12
<i>DSLR Camera Photogrammetry.....</i>	<i>13</i>
<i>3D Scanning.....</i>	<i>13</i>
<i>Manual Measurements.....</i>	<i>14</i>
<i>Water Displacement.....</i>	<i>14</i>
Limitations and Sources of Error.....	15
<i>Precision of Repeat Interval Stops</i>	<i>15</i>
<i>Model Refinement.....</i>	<i>15</i>
<i>External Geometry Measurements.....</i>	<i>16</i>
<i>Determination of Specimen Ends.....</i>	<i>16</i>
Utilization of Internal Photogrammetry Technique on Soil Specimens	16
Results and Discussion.....	19
Photograph Interval	19
Testing of Internal Photogrammetry System on Soil Specimens.....	20
Conclusions	21
Potential Applications and Future Improvements	22
Acknowledgements	24
References	25
LIST OF TABLES.....	27
LIST OF FIGURES	27

Validation of an Internal Camera Based Volume Determination System for Triaxial Testing

Sean E. Salazar EIT¹, **Leah D. Miramontes**², Adam Barnes³, Michelle L. Bernhardt PhD⁴,
Richard A. Coffman PhD PE PLS⁵

¹Graduate Research Assistant, Department of Civil Engineering,
University of Arkansas, Fayetteville, AR 72701. Email: ssalazar@uark.edu.

**²Undergraduate Research Assistant, Department of Civil Engineering,
University of Arkansas, Fayetteville, AR 72701. Email: ldm002@uark.edu.**

³Geomatics Specialist, Center for Advanced Spatial Technologies,
University of Arkansas, Fayetteville, AR 72701. Email: abarnes@cast.uark.edu.

⁴Assistant Professor, Department of Civil Engineering,
University of Arkansas, Fayetteville, AR 72701. Email: mlberha@uark.edu.

⁵Associate Professor, Department of Civil Engineering,
University of Arkansas, Fayetteville, AR 72701. Email: rick@uark.edu.

Abstract

Accurate strain and volume measurements are critical to phase relationships and strength determination for saturated and unsaturated soils. In recent years, laboratory-based photographic techniques of monitoring soil specimens have become more common. These techniques have been used to reconstruct 3D models and to determine strain and volumetric changes of triaxial specimens. A new technique that utilized digital photographs of the soil specimen, captured from within a triaxial testing cell, was utilized. Photographs were processed using photogrammetry software to reconstruct 3D models of the soil specimens. By placing camera equipment within the cell, the technique eliminated the need to account for optical distortions due to 1) refraction at the confining fluid-cell wall-atmosphere interface, 2) the curvature of the cylindrical cell wall, and 3) the pressure-induced deformation of the cell wall.

As documented herein, the internal photogrammetry approach was validated using analog specimens and triaxial compression and extension tests. Furthermore, the viability of determining total and local strains, volume changes, and total volume at any given stage of testing was evaluated. By comparison with other volume-determination methods, including DSLR camera photogrammetry, 3D scanning, manual measurements and water displacement techniques, an accuracy of the internal photogrammetry technique of 0.13 percent was assessed.

Keywords: Triaxial Testing, Photogrammetry, Volume Measurements

Introduction and Background

Researchers have employed various photograph-based methods to monitor soil specimens during triaxial tests. Specifically, these measurements have enabled one or more of the following: 1) axial and radial dimensions and deformations with time, 2) local and/or total volume measurements, 3) volumetric strain calculations, and 4) shear band characterization. Zhang et al. (2015) tabulated examples and provided a discussion of the various methods that were previously utilized to calculate local and/or total volume of triaxial specimens. Examples included double-wall cell systems, differential pressure transducers, measurements of air and water volume changes (Bishop and Donald 1961, Ng et al. 2002, Leong et al. 2004), displacement sensors (Scholey et al. 1995, Bésuelle and Desrues 2001), proximity sensors (Clayton et al. 1989), laser scanners (Romero et al. 1997, Messerklinger and Springman 2007), digital image analysis (Macari et al. 1997, Sachan and Penumadu 2007), digital image correlation (Bhandari et al. 2012), x-ray computed tomography (Desrues et al. 1996, Viggiani et al. 2004), and photogrammetry (Zhang et al. 2015). Specifically, the methods that were mentioned were divided into two broad categories: photograph-based and non-photograph-based methods. In recent years, the popularity of photograph-based methods has surpassed non-photograph-based methods due to their practicality, cost-effectiveness, and versatility. The limitations of the photograph-based and non-photograph-based approaches were discussed in Salazar and Coffman (2015a) and Salazar et al. (2015); the need for the use of photogrammetry that relied upon internal cameras was presented.

Of the photograph-based triaxial monitoring examples in the literature (Macari et al. 1997, Alshibli and Sture 1999, Alshibli and Al-Hamdan 2001, Gachet et al. 2006, Sachan and Penumadu 2007, Rechenmacher and Medina-Cetina 2007, Uchaipichat et al. 2011, Bhandari et al. 2012, Hormdee et al. 2014, Zhang et al. 2015), only the Zhang et al. (2015) technique utilized photogrammetry to obtain total and local volume changes of triaxial soil specimens. Several advantages were observed by utilizing the photogrammetry techniques; the Zhang et al.

(2015) method overcame the previous limitations of photograph-based measurement techniques (including Digital Image Analysis [DIA], Digital Image Correlation [DIC], and Particle Image Velocimetry [PIV]). Zhang et al. (2015) claimed that the ray-tracing and least-square optimization techniques that were utilized to obtain these corrections enabled errors of no more than 0.25 percent. However, because the photographs were acquired externally (from outside of the cell wall) during the implementation of the Zhang et al. (2015) method, computationally intensive corrections were required to account for optical refraction and cell wall flexure.

As an alternative to the aforementioned methods that utilized externally-acquired photographs, Salazar and Coffman (2015a, 2015b) and Salazar et al. (2015) introduced a photogrammetry method that utilized photographs that were captured from within the triaxial cell. As described in Salazar and Coffman (2015a, 2015b) and Salazar et al. (2015), small board cameras with pinhole apertures were mounted to diametrically opposed towers that were located within the triaxial cell. Due to the confined space within the triaxial cell (11.43-cm [4.5-in.] inside diameter), the field of view of the board cameras was limited. Therefore, ten camera devices (five devices stacked vertically on each tower) were required to ensure full photographic coverage of a soil specimen. The towers were mounted on a guided track that allowed for rotation around the soil specimen between the two top cap drainage lines. With the aid of two pairs of magnets (located on the towers and outside of the cell), the towers were manually rotated and stopped at prescribed intervals. Ten photographs were captured at each interval. Photogrammetry software (*PhotoModeler Scanner 2015* [Eos Systems, Inc. 2015]) was then utilized to reconstruct the surface for any soil specimen at any given stage during triaxial testing.

The internal cell photogrammetry system was designed to withstand exposure to the confining fluid (silicone oil) and the typical high confining pressures associated with a triaxial test (up to 1,035 kPa). The primary advantage of the Salazar and Coffman (2015a, 2015b) and Salazar et al. (2015) technique was direct observation of the soil specimen during testing; the

necessity to account for the refraction of light at the confining fluid-cell wall and cell wall-atmosphere interfaces, or the curvature of the cell wall, was therefore eliminated.

The procedures utilized to validate the internal photogrammetry technique are described in *Validation of the Internal Photogrammetry Technique*. The technique was validated using soil analog specimens (brass and two acrylic specimens). The brass specimen and a large acrylic specimen were utilized to examine the effect of the number of photographs (ranging from 40 to 320 photographs) on the photogrammetric derivation of camera locations and on the determination of specimen volume. A small acrylic specimen was utilized to verify the accuracy of the photogrammetric procedures. Furthermore, a discussion of the limitations of the presented technique is included. The procedures for triaxial testing of soil specimens are described in the *Utilization of the Internal Photogrammetry Technique on Soil Specimens* section. Specifically, the methods and materials that were employed to acquire and to process data are included. Results from the triaxial tests are presented in the *Results and Discussion* section. The results were used to demonstrate the viability of the internal photogrammetry approach and to provide visual representation of total and local deformations on the surface of the soil specimens during testing. Discussions of the potential applications and improvements of the internal photogrammetry technique are presented in the *Potential Applications and Future Improvements* section, followed by concluding remarks.

Validation of the Internal Photogrammetry Technique

As discussed herein, the performance of the internal cell photogrammetry approach that was described in Salazar and Coffman (2015a, 2015b) and Salazar et al. (2015) was validated by conducting a series of tests using soil analog specimens (brass and acrylic specimens). Specifically, each step of the approach was validated prior to triaxial compression and extension testing. These steps included 1) the calibration of each of the individual board cameras, 2) the derivation of camera locations and orientations, 3) the determination of suitable photograph-capturing intervals, 4) the capture of photographs of the acrylic analog specimen, 5) the

photogrammetric reconstruction of the acrylic analog specimen, 6) the determination of the volume of the acrylic analog specimen, and 7) the evaluation of the accuracy of the volume determination method. To illustrate the full validation process, a flow chart is presented (Figure 1). As a subset of Figure 1, the photogrammetric processes are further described in in Figure 2.

Calibration of Board Cameras

The camera calibration, as used to determine the intrinsic parameters that describe the internal geometry of the camera, is critical to the application of the principles of photogrammetry. Therefore, each of the ten board cameras was calibrated utilizing the single-sheet calibration procedure, as outlined by Eos Systems, Inc. (2015). Through this method, each of the ten cameras was used to capture photographs of a calibration grid from different perspectives. These photographs were then processed within the *PhotoModeler Scanner 2015* software (herein after referred to as *PhotoModeler*) to derive the intrinsic camera parameters for each of the ten cameras, namely the focal length (f), the sensor format size ($w:h$), and the principal point ($x:y$). These intrinsic camera parameters were imported into all future *PhotoModeler* projects that used any board camera acquired photographs.

Derivation of Camera Locations and Orientations within the Triaxial Cell

In photogrammetry applications, it is necessary to derive the extrinsic parameters for each camera position used to capture a photograph (namely location and orientation in 3D space). To derive this information for the board cameras that were internal to the triaxial cell, the following approach was conducted. A cylindrical, brass analog specimen (38.1mm [1.5in.] diameter by 76.2mm [3.0in.] length, nominal) was wrapped with a sequence of black ringed automatically detected (RAD) coded targets that were printed onto a sheet of white paper (to provide contrast). The brass specimen was then placed upright on a flat surface. Other targets were placed on the flat surface adjacent to the specimen to provide additional tie points, and to increase redundancy and the overall accuracy of the measured target locations on the specimen surface. These additional tie points were also used for datum definition, namely

model orientation and scale. A digital single lens reflex (DSLR) camera (21.2 Megapixel Canon 5D Mark II with fixed 28mm Nikkor lens) was then calibrated using the same procedures that were used to calibrate the board cameras (as previously discussed). The DSLR camera was then employed to capture photographs of all sides of the brass specimen (approximately 40 photographs total). A selection of the photographs were processed using *PhotoModeler* software to identify and locate each target on the surface of the specimen. External geometry measurements acquired using a caliper (distance between several targets within the photographs) were input into the software program to define scale. For reference, the resulting control point cloud of coded target locations (286 target locations total) was saved and imported into all succeeding projects.

The same targeted brass specimen, as previously used, was placed within the instrumented triaxial cell. Photographs of the specimen were captured at every five degrees of rotation around the specimen, with two 20-degree gaps, due to the presence of the two diametrically opposed drain lines (connected to the specimen top cap) on each side of the specimen. The five-degree interval photographs (total of 320 photographs) were analyzed using the *PhotoModeler* software while utilizing the imported control point cloud as a reference. Targets within the newly acquired photographs were identified and assigned to the corresponding locations of the imported control points. The software was then utilized to derive the location (X, Y, Z) and orientation (Omega, Phi, Kappa) of each of the individual board cameras at each interval. These virtual camera locations and orientations corresponded to the photograph interval stops around the specimen within the instrumented cell. Therefore, all future photograph acquisitions were assigned to the respective photogrammetrically-derived camera locations and camera orientations.

Determination of Photograph-Capturing Intervals

Given the constraints of close-range photogrammetry, and to allow for full photographic coverage of the surface of a specimen, it was necessary to capture photographs at intervals of

rotation about the specimen. It was desired to minimize the number of photographs required to reconstruct the specimen, while maintaining a high degree of accuracy and precision. Furthermore, the accuracy of the location of a point was influenced by the angle between photographs (perspective). It was therefore desired to optimize the angle between photographs while maintaining photograph redundancy (overlap) in adjacent photographs. Furthermore, a sensitivity study was performed to determine the ideal angle between adjacent sets of photographs. The study was conducted by placing a different analog specimen (acrylic, 44.5mm [1.75in.] diameter by 88.9mm [3.5in.] length, nominal) into the instrumented triaxial cell and capturing photographs of the specimen at five degree intervals (320 photographs, total). The larger specimen was selected because it represented the maximum dimensions that would be achieved during large-strain triaxial compression (maximum diameter) or extension (maximum height) tests on actual soil specimens. The cell remained empty (air, instead of confining fluid) for this stage of the validation process. The sensitivity of the camera locations to the angle between the photograph capturing intervals was evaluated for 45-, 30-, 15-, and five-degree intervals, which corresponded to 40, 60, 110, and 320 photographs, respectively. These intervals were chosen because each interval was divisible by the next, allowing for one common photoset to be used.

Capture of Photographs of Acrylic Specimen

The same procedures that were utilized to 1) derive the board camera locations and orientations using the brass analog specimen (in air) and to 2) determine the ideal angle between photos using the large, acrylic analog specimen (also in air) were employed to validate the method using a second, smaller acrylic analog specimen (38.1mm [1.5in.] diameter by 76.2mm [3.0in.] length, nominal) submerged in confining fluid (silicone oil) within the triaxial cell. The same sequence of unique RAD-coded targets (that were utilized previously to wrap the brass specimen) were adhered to the surface of the acrylic specimen after the targets had been printed onto a sheet of temporary tattoo adhesive paper. 1) Like with the brass specimen, the

DSLR camera was again used to photograph the specimen (in air, on a flat surface), 2) a control point cloud of coded target locations was created, 3) photographs of the specimen were captured from within the instrumented triaxial cell (this time in confining fluid), 4) photographs were processed using *PhotoModeler* software, and 5) camera locations and orientations within the silicone oil filled triaxial cell were derived.

The coded targets that were adhered to the surface of the acrylic specimen were removed and a different sequence of coded targets was adhered to the surface of the specimen using the temporary tattoo adhesive paper. A different sequence of targets was used because it distinguished them from the targets that were already identified to create the control point cloud (used to derive the camera locations and orientations). The acrylic specimen was then placed within the triaxial cell filled with confining fluid once more and photographs were captured to reconstruct the specimen. This second set of photographs of the acrylic specimen was necessary because it would not have been a fair assessment to derive the target locations on the surface of the specimen using the same photographs that were utilized to derive the camera locations and orientations.

Photogrammetric Reconstruction of a Specimen

The photographs of the two acrylic analog specimens (large specimen used to evaluate photograph capturing interval and smaller specimen used to validate technique when subjected to the confining fluid) that were captured from within the triaxial cell were processed within *PhotoModeler* software to photogrammetrically reconstruct the specimens. The photogrammetry projects that were created during the camera location and orientation step were modified by replacing the photographs within the projects with the newly acquired photographs of the acrylic specimens. This ensured that the geometric constraints (camera location and orientation) remained constant, thereby enabling the greatest possible accuracy for the close-range photogrammetry technique. The control points (that were created in the camera location and orientation projects) remained in place, but their visibility was disabled to reduce confusion while

the locations of the new targets were being measured. Targets on the surface of the acrylic specimens were identified in at least three photographs and assigned to their respective unique identification numbers (384 and 283 total targets total for large- and small-acrylic specimens, respectively). Three-dimensional coordinates were then automatically assigned to each commonly referenced point in the project. The circular centers of the targets provided a reliable means of identifying the precise locations of the targets. To aid in the reliable identification of common points on the ends of the specimen, high contrast markers were added to the porous stones on both ends of the specimen. The intersections between the markers, the porous stones, and the ends of the specimen served to identify common points along the ends of the specimen. Internal quality feedback within the *PhotoModeler* software aided in identifying and reducing point measurement errors, thereby 1) ensuring the quality of the photogrammetry projects and 2) providing consistency among each of the projects that were processed. The quality feedback metrics included total error, residuals, and point precision values.

After all of the points on the surfaces of the specimens were identified, radial curves were drawn through the 3D points on the surface of the virtual specimens. Surface tools were utilized to create outward-facing surfaces on the specimens; these surfaces were created by using the curves as the edges of each surface, and to cap the open ends of the specimens. The virtual specimens therefore took shape using the newly created surfaces; however, the *PhotoModeler* software did not correctly calculate the internal volumes of the virtual specimens, nor were the surfaces “watertight”. The 3D models were therefore exported in a wavefront format (.obj extension) to allow for further analysis using a software program that was more suited to determining the accurate volume of a virtual object. The *Geomagic Design X* software package (3D Systems, Inc. 2015) was utilized for this purpose.

Determination of a Specimen Volume

Each 3D model exported from *PhotoModeler* consisted of a number of disconnected polygonal bands wrapped transversely around the surface of the model. Narrow gaps between

these polygonal bands were sealed using the *Global Remesh* and *Healing Wizard* tools within the *Geomagic Design* software. The *Global Remesh* tool worked by essentially shrink-wrapping the 3D model with a new, improved surface that was free of holes, slivers, and other topologic imperfections. The settings for this tool were adjusted so that the number of polygons that made up the output model was 100 times the number of polygons of the input model. The increase in the quantity of polygons reduced the potential for rounding that was observed along sharp edges. Moreover, the *Healing Wizard* was then used to detect and remove any small clusters of free-floating polygons that were not actually part of the surface of the models. After the final watertight models were created, the calculation of the volume of each model was revealed when selecting on the properties of the model.

Evaluation of Accuracy of Technique

To evaluate the accuracy of the internal cell photogrammetry approach that is presented herein, several other techniques were also employed to determine the volume of the smaller acrylic analog specimen. The techniques included 1) the aforementioned internal photogrammetry technique (within triaxial cell), 2) photogrammetry using DSLR camera obtained photographs only (external, not within the triaxial device), 3) a 3D scanning technique, 4) manual measurements using a caliper and pi tape, and 5) a water-displacement technique. Based on a review of the literature, no universal method exists to evaluate the absolute or “true” accuracy of a volume determination technique. The amount of difference relative to an external reference, often termed “error”, is only meaningful when the nature of the external reference is reported. To provide a metric for comparison between the volumes of the smaller acrylic specimen, as obtained using each technique, the difference was evaluated relative to the water displacement technique. This technique was selected, because it was based on well-established procedures documented in ASTM D698 (2014) to determine the interior volume of a Proctor mold.

DSLR Camera Photogrammetry

For the DSLR camera survey technique, the smaller acrylic specimen was placed on a table and approximately 40 photographs were captured of the specimen from various angles. The photographs were imported into *PhotoModeler* software and a selection of the photos were processed. Common points (coded targets) on the surface of the specimen were identified and referenced to ensure that they appeared in at least three photos. Measurements were imported to define the scale (known distance between select points) and orientation (x, y, and z axes). Similar to the internal photogrammetry technique, surfaces were created on the virtual specimen in *PhotoModeler* and the model was exported for processing and analysis within the *Geomagic Design* software.

3D Scanning

By definition, 3D scanning is the use of a specialized instrument to rapidly record the 3D information of an object or environment. The *Breuckmann SmartScan3D HE* was employed to obtain the 3D data of the acrylic specimen. This device is a close range 3D digitizing system that utilized fringe projection or structured white light technology. Specifically, a projector, two 5-Megapixel color cameras, and multiple lenses were utilized to facilitate the 3D measurements. A series of patterns (or fringes) were cast onto the specimen and the difference in the pattern from each camera was utilized to compute a series of discrete measurements or 3D points. The *SmartScan3D HE* instrument captured approximately 150,000 points per individual scan.

The smaller acrylic specimen was scanned with the *SmartScan3D HE* and a set of M-125 lenses (i.e. 125 mm diagonal field-of-view at the optimal working distance of one meter). The M-125 lenses, the highest resolution lenses available for this scanner, were used to achieve the highest possible spatial resolution of approximately 60 μm horizontal. To begin the process of scanning, the instrument was calibrated using 1) the prescribed procedure that was recommended by the manufacturer, 2) a set of calibration targets, and 3) the *OPTOCAT 2013 R2* software. The calibration procedure reported an average accuracy of object points of 15.41

μm in the X, $0.74 \mu\text{m}$ in the Y, and $26.75 \mu\text{m}$ in the Z dimension (depth from scanner). The specimen was made of an acrylic material that is partially transparent; to prevent scan errors caused by light scattering during fringe projection, a thin coat of matte white spray paint was applied to the specimen. Several spherical adhesive targets were also placed on each side of the specimen to aid in the scan-to-scan alignment procedures during data processing. The specimen was then placed at a 45-degree angle on an automated turntable (Figure 3) and scanned at 20-degree intervals for a total of 18 scans. Two other manually positioned scans were collected to fill in areas not visible during the turntable rotations. All of these data (20 scans) were then processed using the OPTOCAT software. The basic processing steps that were performed included: 1) an iterative global best-fit alignment of all scans, 2) overlap reduction to remove scan data collected at a high angle of incidence, 3) merging of individual scans to create a single polygonal mesh, 4) smoothing to remove small amounts of noise and other scan artifacts, and 5) hole-filling using the semi-automated tools that were available. The final 3D model, as presented in Figure 3, was composed of approximately 685,000 polygonal faces and approximately 343,000 vertices.

Manual Measurements

For the manual measurements method, a linear caliper (with a resolution of 0.05 mm) was utilized to measure the length of the acrylic specimen (average of three measurements) and a pi tape (with a resolution of 0.01 mm) was used to measure the diameter of the specimen (average of three measurements). The volume of the specimen was then calculated based on the average measurements.

Water Displacement

The same procedures that are commonly utilized to measure the volume of a Proctor mold (ASTM D698 2014) were used to measure the volume of the specimen. Specifically, after the volume of a Proctor mold was determined using the water-filling method that is described in the Annex of the ASTM, the specimen was placed into the Proctor mold and submerged in de-

ionized and de-aired water to determine the amount of water that was displaced by the specimen. The mass of the acrylic specimen was determined before and after water submersion to ensure that no water was imbibed by the specimen during the testing.

Limitations and Sources of Error

The limitations of, and the sources of error associated with, the described photogrammetry technique are discussed herein. A schematic of the factors that influence the accuracy of photogrammetry applications is presented as Figure 4. Several sources of error were identified within the presented technique. Therefore, the accumulation of independent sources of error produced an effect that may have propagated the error throughout the process of collecting, processing, and evaluating data. To overcome all of the potential sources of error, each source of error was addressed prior to occurrence.

Precision of Repeat Interval Stops

The camera tower stops at intervals around the specimen were marked on the rotating platform to allow for repeat occupation (during a given photogrammetry project and between successive photogrammetry projects). The method relied upon the capture of photographs from the exact same locations with each repetition, because photographs with known (derived) camera locations and orientations were replaced with new photographs (thereby assigning the derived locations and orientations to the new photographs). Although the same locations were reoccupied for each test, the precision of each reoccupation was only assessed visually. Any deviation from the photogrammetrically derived location resulted in error in the three-dimensional coordinate of an observed point within the replaced photographs.

Model Refinement

The number of targets that were utilized limited the mesh refinement of the surface of each specimen. Furthermore, the number of targets that were utilized was related to processing time and to the minimum size of targets. To maintain the automated target identification capability of the *PhotoModeler* software, a target center diameter of at least 30 pixels was

utilized. This resulted in the use of 286 targets, that were evenly distributed (center to center spacing of 5.65 mm) across the surfaces of the 38.1mm (1.5in.) diameter by 76.2mm (3.0in.) length (nominal) brass and acrylic soil specimens.

External Geometry Measurements

To scale a photogrammetry project, one or more external reference measurements was required to be input. These reference measurements were in the form of a known distance between two measured points located within the project. The resulting overall accuracy of a project was therefore limited to the accuracy of the input measurements. To mitigate the impact of this source of error, multiple reference measurements were made for various target pairs within the project.

Determination of Specimen Ends

The most difficult aspect of processing the photographs of a specimen was the reliable identification of the ends of the specimen (i.e. picking points along the edges at the two ends of the specimen). Picking end points was challenging because distinct markers had to be identified subjectively in adjacent photographs without the help of target centers. This challenge has often been understated or not discussed in the literature, but should not be overlooked. To aid in the reliable identification of specimen ends, high contrast markers were applied to the porous stones on the ends of the specimens.

Utilization of Internal Photogrammetry Technique on Soil Specimens

Two triaxial tests were performed on kaolinite soil specimens to assess the viability of determining total and local strains, total volume and volume changes at any given stage of testing, and the actual failure plane of a soil specimen. Specifically, one undrained, conventional triaxial compression (CTC) test and one undrained, reduced triaxial extension (RTE) test were performed. As an example, a schematic of the stages of a typical compression test is presented as Figure 5. In a typical triaxial compression test, the exact total specimen volume at any given stage of testing (prior to consolidation, prior to shearing, or during shearing), must be back-

calculated from testing and post-testing data using phase relationships and assumptions (most notably the right circular cylinder assumption). This method of calculating specimen volume often leads to erroneous results without any means of verification. The internal photogrammetry system provided a means of directly and accurately determining the volume of a soil specimen at any desired stage of testing without the need to rely upon erroneous assumptions during back-calculations.

Soil specimens consisted of commercially available kaolinite soil, *Kaowhite-S*, obtained from the Thiele Company (Sandersonville, Georgia). The specimens were slurry-consolidated in an acrylic consolidometer under an overburden stress of 138 kPa (20 psi). Specimens with nominal dimensions of 7.62-cm length and 3.81-cm diameter were extracted from the consolidation apparatus and weighed. Using temporary tattoo paper, RAD-coded targets were applied to the surface of the first membrane. The membrane was then placed onto the specimen, and a second membrane was applied over the first membrane (to reduce the potential for liquid transfer or gas permeation). During the specimen preparation phase, care was taken to minimize the amount of disturbance on the soil specimen. The top and bottom drain lines to the specimen were flushed to remove air from the lines and the specimen was back pressure saturated (B-check equal to 0.95 or higher) before proceeding to the consolidation phase. During each test, the specimen was consolidated under K_0 -conditions to a vertical effective stress of 310 kPa (45 psi). Upon completion of consolidation, the drain lines were closed and the specimen was sheared under undrained conditions (strain rate of 0.5 percent per hour). For the CTC test, the shearing was paused at intervals of 0, 2, 4, 6, 8, 11.5, and 15 percent strain. At each of these strain intervals, ten photographs of the specimen were captured at 20-degree photograph intervals (total of 80 photographs per strain interval). Similarly, for the RTE test, the shearing was paused at intervals of -0, -2, -4, -6, -8, -10, -12, -15 percent strain and photographs of the specimen were captured. For completeness, a photograph of the instrumented triaxial cell, as utilized in the RTE test, is presented (Figure 6).

Processing procedures were identical to those employed to model the acrylic analog specimen. After 3D models of the soil specimens were exported to wavefront format files, the models were further analyzed within *Geomagic Design* software. Local displacements on the surface of each soil specimen were visualized using the built-in *Mesh Deviation* function. Utilization of this function allowed for two watertight meshes to be overlaid (onto common coordinates) to compare the positive or negative changes between the surfaces of the two meshes. A color-graded scale was selected to visualize the magnitude of changes (cooler colors corresponded to negative changes while warmer colors correlated to positive changes).

In addition to the triaxial compression and triaxial extension tests, one additional unconfined compression (UC) test was performed. The purpose of the UC test was to compare 1) the calculated volumes during a test within the triaxial cell by utilizing the internal photogrammetry technique, with 2) the calculated volumes during a test outside of the triaxial cell utilizing the DSLR camera photogrammetry technique. The soil specimen was prepared in an identical way to those specimens that were used in the triaxial tests. RAD-coded targets were applied to the surface of the membrane and additional targets were placed on the loading frame around the specimen to provide tie points for photogrammetric processing. The specimen was sheared under unconfined conditions (although the specimen was wrapped in a membrane) at a strain rate of 0.5 percent per hour. During the test, the shearing was paused at intervals of 0, 2, 4, 6, 8, 11.5, and 15 percent axial strain and approximately 40 photographs of the specimen were captured at each strain interval. During the processing phase, 12 photos of the 40 photos that were captured for each strain interval, were selected and processed so that targets on the surface of the specimen appeared in at least three photographs. Following the same procedures as those used for the internal photogrammetry technique, 3D models were created within *PhotoModeler* software and were exported for further analysis within *Geomagic Design* software.

Results and Discussion

The results from the validation of the internal cell photogrammetry technique are presented herein. Furthermore, a discussion of the amount of error associated with the technique and the sensitivity of the photograph-capturing interval are presented. The accuracy of the utilized photogrammetry technique is discussed and the limitations are highlighted.

As presented in Table 1, the differences of the various volume measurement techniques relative to the reference (water displacement technique) fell within one-half of one percent. These difference values were expected to be greater for the techniques presented herein than the difference values reported in the literature. This was expected because of the relatively small size of the specimens that were utilized for validation of the internal photogrammetry technique (nominal dimensions of 7.62-cm length and 3.81-cm diameter), as compared to larger size specimens contained within the literature (typically, 10.16-cm length and 5.08-cm diameter, or 14.22-cm length and 7.11-cm diameter). The smaller specimen size was utilized because of the reduced drainage distance, which significantly reduced the time required for the completion of the consolidation phase of testing.

Photograph Interval

Although it appeared that derived camera location difference was sensitive to the photograph interval (degree of separation between sets of photographs), as indicated by convergence of camera locations in Figure 7, the effect was considered negligible (within 0.045 pixels for the maximum difference in camera location). The relationship between derived camera location and photograph interval was not directly meaningful. Therefore, the influence of the photograph interval on the determination of specimen volume was examined (Table 2). For the volume (as calculated from four photogrammetric reconstructions, using 45, 30, 15, and 5 degree photograph intervals), the standard deviation was equal to 0.34 cm³, and the range was equal to 0.70 cm³. The determination of volume was therefore not sensitive to the photograph interval. Thus, to 1) match the 20-degree gaps surrounding the drain tubes within the triaxial cell

and 2) provide consistent photograph intervals, an interval of 20 degrees was selected. This resulted in 80 photographs and approximately 280 minutes of processing time per photogrammetry project.

Testing of Internal Photogrammetry System on Soil Specimens

The volume of the soil specimens was determined at various levels of axial strain during both the CTC and RTE tests, as well as during the UC test. The CTC and RTE tests were performed in an undrained condition and therefore the total volume of the specimen was not expected to change during the shearing phase of each test. Likewise, the UC test was undrained. The volumes that were measured during each test, and the summary statistics for each test, support this hypothesis. The results from the CTC test are presented in Table 3. The volume change during the consolidation phase was determined to be 6.56 cm^3 , using the internal photogrammetry technique. As a comparison, the volume change determined from the pore pump was equal to 6.81 cm^3 (temperature corrected) and the change calculated from the displacement transducer was equal to 6.70 cm^3 (using the assumption that the cross-sectional area of the specimen remained constant during K_0 consolidation). The internal photogrammetry approach therefore underpredicted the volume change by 3.7 percent, as compared to the pump measurements, and by 2.1 percent, as compared to calculations using the change in specimen height.

The results from the RTE test and the UC test are presented in Table 4 and Table 5, respectively. For the CTC, RTE, and UC tests, the small changes in total volume, during undrained shearing, were likely a result of the sensitivity to limited refinement of the 3D model surface (function of the number of targets on the membrane). As indicated by the standard deviation of total volumes calculated during the CTC test (0.37 cm^3), as compared to the standard deviation during the RTE test (0.27 cm^3), the variability was greater for the CTC test. The likely cause of the greater variability during the CTC test was that the target refinement was more sensitive to the local deformations on the surface of the specimen during compression

(uneven bulging) than during extension (fairly uniform necking). Comparison with the results from the UC test (standard deviation of 0.69 cm^3) revealed that even with the high resolution DSLR camera photogrammetry technique there was variability in the volumes, further supporting the hypothesis that the model refinement (number and density of targets on surface of the specimen) affected the accurate determination of specimen volume throughout a test.

The localized displacements of each specimen were visualized qualitatively for the CTC and RTE tests. Specifically, the displacements were visualized for the consolidation phase of testing, as presented in Figure 8, and for the shearing phase, as presented in Figure 9. During the consolidation phase, the small strains in the radial direction of the specimen were somewhat unexpected, as the triaxial testing apparatus was programmed for K_0 -consolidation by which the diameter of the specimen should have remained constant throughout the consolidation phase of the test. In the CTC test (Figure 9a), the actual failure plane of the soil specimen was evident from the shear banding behavior at larger strains (greater than eight percent axial strain). Conversely, necking behavior was observed for the specimen in the RTE test (Figure 9b).

Conclusions

The internal cell photogrammetry technique that was previously described was validated to determine the volume of soil specimens during all stages of triaxial compression (CTC) and triaxial extension (RTE) tests. Specifically, the technique was successfully employed to monitor the volume of kaolinite soil specimens during undrained, conventional, triaxial compression and undrained, reduced, triaxial extension tests. The novel camera instrumentation, internal to the triaxial cell wall, allowed for direct observation of the entire surface of the soil specimens throughout the triaxial tests. The necessary assumptions and cumbersome corrections for refraction were eliminated, thereby improving upon externally-acquired photograph-based methods that have been recommended in the literature. The principles of close-range photogrammetry were utilized to enable accurate 3D reconstructions of the soil specimens. Prior to triaxial testing, a variety of outside-of-cell volume determination techniques, including DSLR

camera photogrammetry, 3D scanning, manual measurements, and water displacement techniques were employed to provide comparisons for the volume of an acrylic analog specimen as determined utilizing the internal cell photogrammetry technique. Results from the internal photogrammetry technique fell within 0.13 percent of the reference technique and results from all comparison techniques fell within 0.50 percent. To minimize processing time to approximately 280 minutes, a balance was struck between the number of photographs utilized (80) and the reliability in photogrammetric measurements. 3D models were produced using commercially available software and localized displacements that developed during the triaxial testing were visualized and reported.

Potential Applications and Future Improvements

There are several potential applications for using the internal photogrammetry system. The approach may be utilized to provide verification of axial and radial strain measurements at any point on the surface of the specimen or at the end cap connection. Furthermore, the strain-based approach could be used in conjunction with 3D finite element analysis techniques to predict the stress distribution throughout the specimen. This inverse solution will aid in developing understanding into the constitutive models of the soil behavior.

Future improvements to the internal photogrammetry system may facilitate increased accuracy of the results. A higher degree of precision, in the reoccupation of photograph interval stops around the specimen, would reduce the error associated with the processing of photogrammetry projects. Therefore, a mechanized rotating track base is recommended for future applications. Furthermore, future projects may also incorporate a geometric constraint that allows some small amount of deviation from the known camera positions, but only along a modeled arc representing the circular path of the camera track.

To increase the level of refinement on the surface of a specimen, a greater number of targets may be required. However, the size of (and therefore the number of) the targets that were utilized was limited, due to the resolution of the modified board camera devices. To reduce

the approximations between targets, improved camera resolution will allow for denser target coverage on the specimen surface. Furthermore, improvements in automatic target identification algorithms will result in reduced time required for processing.

Acknowledgements

*This material is based upon work supported by the National Science Foundation Graduate Research Fellowship under Grant No. DGE-1450079, as awarded to S.E. Salazar. The authors would also like to acknowledge the following support: 1) **University of Arkansas Honor College Research Grant, awarded to L.D. Miramontes under the mentorship of R.A. Coffman.** 2) **University of Arkansas Provost Collaborative Research Grant, awarded to R.A. Coffman (PI), M.L. Bernhardt (Co-PI) and A. Barnes (Co-PI).** 3) **United States Department of Transportation (USDOT) Office of the Assistant Secretary for Research and Technology (OST-R) under Research and Innovation Technology Administration (RITA) Cooperative Agreement Award No. OASRTRS-14-H-UARK awarded to R.A. Coffman (PI) and T. Oommen (Co-PI).** The views, opinions, findings, and conclusions reflected in this manuscript are the responsibility of the authors only and do not represent the official policy or position of the USDOT/OST-R, or any state or other entity.*

References

- Alshibli, K. A., and Sture, S. 1999. Sand shear band thickness measurements by digital imaging techniques. *Journal of Computing in Civil Engineering*, **13**(2): 103-109.
- Alshibli, K. A., and Al-Hamdan, M. Z. 2001. Estimating volume change of triaxial soil specimens from planar images. *Computer-Aided Civil and Infrastructure Engineering*, **16**(6): 415–421.
- American Society for Testing and Materials. 2014. Standard test methods for laboratory compaction characteristics of soil using standard effort. *Annual Book of ASTM Standards, Designation D698, Vol. 4.08*, ASTM, West Conshohocken, Pennsylvania.
- Bésuelle, P., and Desrues, J. 2001. An internal instrumentation for axial and radial strain measurements in triaxial tests. *Geotechnical Testing Journal*, **24**(2): 193-199.
- Bhandari, A.R., Powrie, W., and Harkness, R.M. 2012. A digital image-based deformation measurement system for triaxial tests. *Geotechnical Testing Journal*, **35**(2): 18 pgs.
- Bishop, A.W., and Donald, I.B. 1961. The experimental study of partly saturated soil in triaxial apparatus. *In Proceedings of the Fifth International Conference on Soil Mechanics and Foundation Engineering, Paris, France, 17-22 July 1961*. Dunod, Paris, pp. 13-21.
- Desrues, J., Chambon, R., Mokni M., and Mazerolle, F. 1996. Void ratio evolution inside shear bands in triaxial sand specimens studied by computed tomography. *Géotechnique*, **46**(35): 529-546.
- Eos Systems, Inc. 2015. *PhotoModeler Scanner* (Version 2015.0.0). 3D Measurements and Models Software. Vancouver, British Columbia.
- Gachet, P., Geiser, F., Laloui, L., and Vulliet, L. 2007. Automated digital image processing for volume change measurement in triaxial cells. *Geotechnical Testing Journal*, **30**(2): 98-103.
- 3D Systems, Inc. 2015. *Geomagic Design X* (Version 17). 3D Computer-Aided Design (CAD) Software. Rock Hill, South Carolina.
- Hormdee, D., Kaikeerati, N., and Jirawattana, P. 2014. Application of image processing for volume measurement in multistage triaxial tests. *Advanced Materials Research*, **931-932**: 501-505.
- Leong, E.C., Agus, S.S., and Rahardjo, H. 2004. Volume change measurement of soil specimen in triaxial test. *Geotechnical Testing Journal*, **27**(1): 10 pgs.
- Macari, E.J., Parker, J.K., and Costes, N.C. 1997. Measurement of volume changes in triaxial tests using digital imaging techniques. *Geotechnical Testing Journal*, **20**(1): 103–109.
- Messerklinger, S., and Springman, S.M. 2007. Local radial displacement measurements of soil specimens in a triaxial test apparatus using laser transducers. *Geotechnical Testing Journal*, **30**(6): 12 pgs.
- Ng, C.W.W., Zhan, L.T., and Cui, Y.J. 2002. A new simple system for measuring volume changes in unsaturated soils. *Canadian Geotechnical Journal*, **39**(3): 757-764.

Rechenmacher, A.L. and Medina-Cetina, Z. (2007). "Calibration of Soil Constitutive Models with Spatially Varying Parameters." *Journal of Geotechnical and Geoenvironmental Engineering*, Vol. 133, No. 12, pp. 1567–1576.

Romero, E., Facio, J.A., Lloret, A., Gens, A., and Alonso E.E. 1997. A new suction and temperature controlled triaxial apparatus. *In Proceedings of the 14th International Conference on Soil Mechanics and Foundation Engineering*, Hamburg, Germany, 6-12 September 1997. August Aimé Balkema, Amsterdam, pp. 185-188.

Sachan, A. and Penumadu, D. 2007. Strain localization in solid cylindrical clay specimens using digital image analysis (DIA) technique. *Soils and Foundations*, **47**(1): 67-78.

Salazar, S.E., Barnes, A., and Coffman, R.A. 2015. Development of an internal camera based volume determination system for triaxial testing. *Geotechnical Testing Journal*, **38**(4): 11 pgs.

Salazar, S.E., and Coffman, R.A. 2015a. Consideration of internal board camera optics for triaxial testing applications. *Geotechnical Testing Journal*, **38**(1): 11 pgs.

Salazar, S.E., and Coffman, R.A., 2015b. Discussion of "A photogrammetry-based method to measure total and local volume changes of unsaturated soils during triaxial testing" by Zhang et al. (doi: 10.1007/s11440-014-0346-8)" *Acta Geotechnica*. doi: 10.1007/s11440-015-0380-1.

Scholey, G.K., Frost, J.D., Lo Presti, C.F., and Jamiolkowski, M. 1995. A review of instrumentation for measuring small strains during triaxial testing of soil specimens. *Geotechnical Testing Journal*, **18**(2): 137–156.

Uchaipichat, A., Khalili, N., and Zargarbashi, S. 2011. A temperature controlled triaxial apparatus for testing unsaturated soils. *Geotechnical Testing Journal*, **34**(5): 9 pgs.

Viggiani G., Lenoir N., Bésuelle P., Di Michiel M., Marellò S., Desrues J., and Kretzschmer M. 2004. X-ray microtomography for studying localized deformation in fine-grained geomaterials under triaxial compression. *Comptes rendus de l'Académie des sciences, série IIb, Mécanique/Mechanics*, **332**: 819-826.

Zhang, X., Li, L., Chen, G., and Lytton, R. 2015. A photogrammetry-based method to measure total and local volume changes of unsaturated soils during triaxial testing." *Acta Geotechnica*, **10**(1): 55-82. doi: 10.1007/s11440-014-0346-8.

LIST OF TABLES

Table 1. Comparison of small-acrylic analog specimen volumes as obtained using five different techniques.

Table 2. Comparison of large-acrylic analog specimen volumes as determined during internal photograph interval sensitivity test.

Table 3. Volumes of kaolinite soil specimen as determined throughout the triaxial compression test and corresponding summary statistics.

Table 4. Volumes of kaolinite soil specimen as determined throughout the triaxial extension test and corresponding summary statistics.

Table 5. Volumes of kaolinite soil specimen as determined throughout the unconfined compression test and corresponding summary statistics.

LIST OF FIGURES

Figure 1. The process used to validate internal cell photogrammetry and to obtain test parameters.

Figure 2. The process used to determine the volume of a specimen using internal cell cameras and the sensitivity of photograph interval on the volume of the specimen.

Figure 3. *a)* Photograph of, and *b)* three-dimensional, watertight model of small-acrylic analog specimen with spherical adhesive targets (removed during processing), as obtained during 3D scanning of specimen.

Figure 4. Factors affecting accuracy in photogrammetry (modified from Eos Systems, Inc. 2015).

Figure 5. Typical measurements and calculations required for conventional triaxial compression test to determine phase diagram of soil specimen during test.

Figure 6. Photograph of the kaolinite specimen within the photogrammetrically instrumented triaxial cell during the shearing stage of the extension test.

Figure 7. Derived camera location difference as a function of photograph interval.

Figure 8. Strain visualization of photogrammetry-obtained, three-dimensional models of kaolinite specimen during consolidation phase of triaxial test (warm colors indicate positive deformation and cool colors indicate negative deformation).

Figure 9. Strain visualization of photogrammetry-obtained, three-dimensional models of kaolinite test specimen during *a)* conventional triaxial compression, and *b)* reduced triaxial extension tests up to 15 percent axial strain during shearing (warm colors indicate positive deformation and cool colors indicate negative deformation).

Table 1. Comparison of small-acrylic analog specimen volumes as obtained using five different techniques.

Volume Determination Method	Volume of Specimen [cm ³]			Mean [cm ³]	Difference from Reference [%]
	Repetition				
	1	2	3		
Water Displacement	94.97	95.60	95.47	95.35	Reference
Manual Measurements	95.82	95.82	95.82	95.82	0.50
3-D Scan	95.64	-	-	95.64	0.31
DSLR Photogrammetry	95.62	-	-	95.62	0.29
Internal Photogrammetry	95.22	-	-	95.22	-0.13

Table 2. Comparison of large-acrylic analog specimen volumes as determined during internal photograph interval sensitivity test.

Rotation Interval [Degrees]	Number of Photos	Computational Cost [minutes]	Specimen Volume V_T, [cm³]	Summary Statistics	
45	40	120	135.17	Mean Volume [cm ³]	135.56
30	60	180	135.37	Standard Deviation [cm ³]	0.34
15	110	330	135.87	Standard Error [cm ³]	0.17
5	320	960	135.80	Coefficient of Variation [%]	0.25
				Range [cm ³]	0.70

Note: Photographs acquired using internal board cameras.

Table 3. Volumes of kaolinite soil specimen as determined throughout the triaxial compression test and corresponding summary statistics.

Testing Phase	Axial Strain ϵ_a, [%]	Volume V_T, [cm³]	Summary Statistics	
Consolidation	Pre-consolidation	89.72	Change in Volume During Consolidation [cm ³]	6.56
	0	83.16		
Shear	2	82.92	Mean Volume During Shear [cm ³]	83.37
	4	83.28		
	6	83.27	Standard Deviation [cm ³]	0.37
	8	83.28	Standard Error [cm ³]	0.14
	11.5	84.10	Coefficient of Variation [%]	0.45
	15	83.55	Range [cm ³]	1.18

Note: Photographs acquired using internal board cameras.

Table 4. Volumes of kaolinite soil specimen as determined throughout the triaxial extension test and corresponding summary statistics.

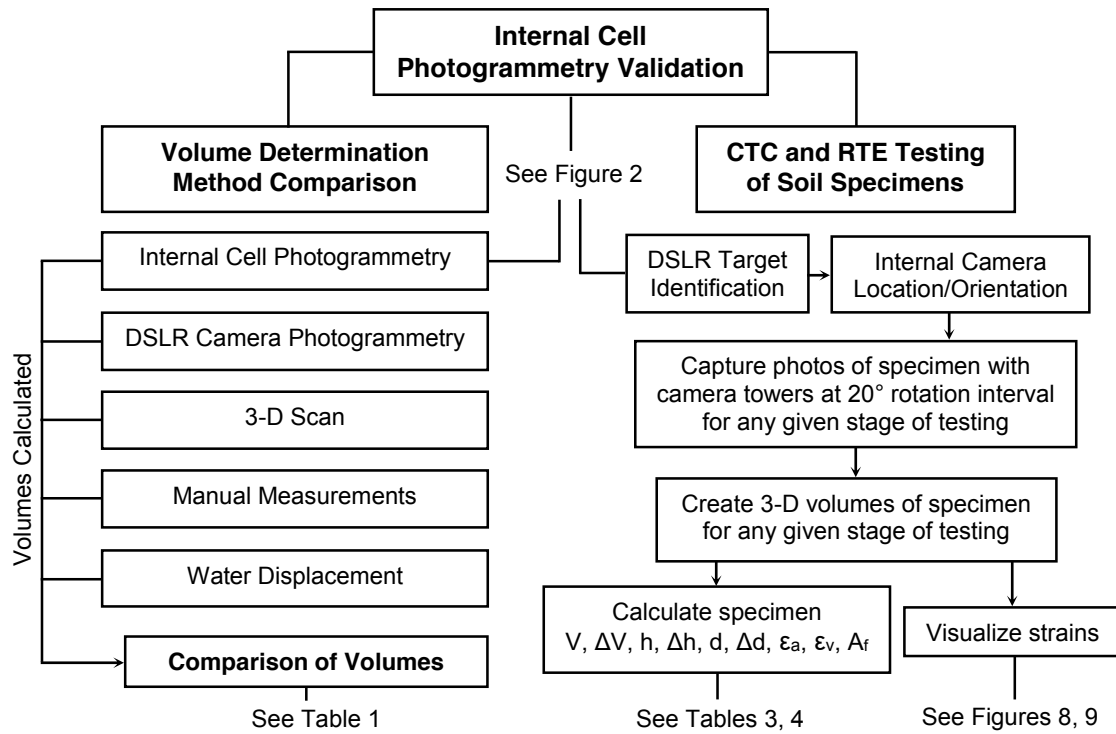
Testing Phase	Axial Strain ϵ_a , [%]	Volume V_T , [cm ³]	Summary Statistics	
Shear	0	79.88	Mean Volume	80.30
	8	80.40	During Shear [cm ³]	
	10	80.32	Standard Deviation [cm ³]	0.27
	12	80.28	Standard Error [cm ³]	0.12
	15	80.64	Coefficient of Variation [%]	0.34
			Range [cm ³]	0.76

Note: Photographs acquired using internal board cameras.

Table 5. Volumes of kaolinite soil specimen as determined throughout the unconfined compression test and corresponding summary statistics.

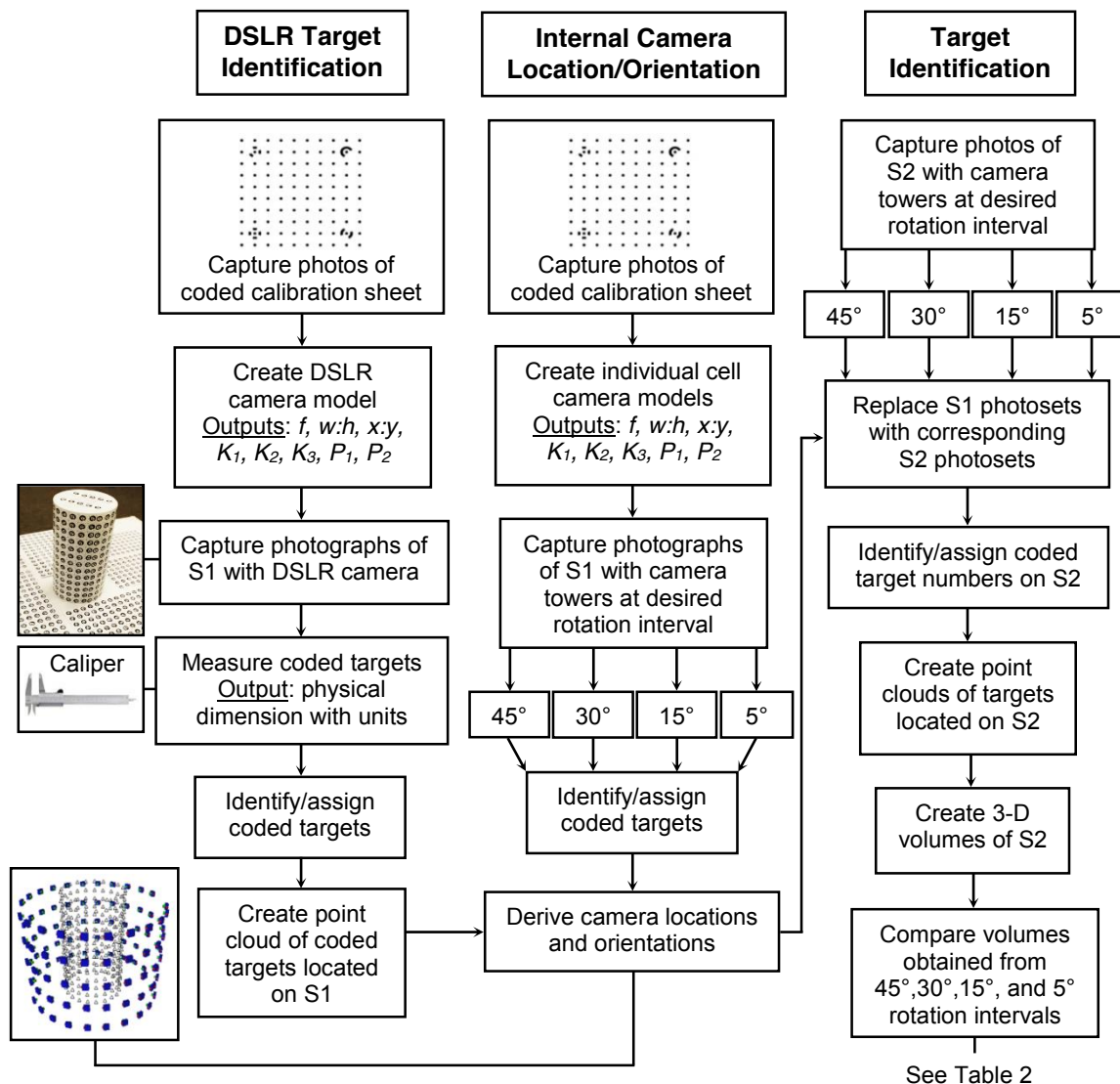
Testing Phase	Axial Strain ϵ_a, [%]	Volume V_T, [cm³]	Summary Statistics	
Shear	0	91.01	Mean Volume	91.35
	2	91.46	During Shear [cm ³]	
	4	90.99	Standard Deviation [cm ³]	0.69
	6	90.90	Standard Error [cm ³]	0.26
	8	90.75	Coefficient of Variation [%]	0.75
	11.5	91.57	Range [cm ³]	2.00
	15	92.75		

Note: Photographs acquired using DSLR camera.



Where DSLR is *digital single lens reflex (camera)*, CTC is *conventional triaxial compression*, RTE is *reduced triaxial extension*, V is volume, ΔV is change in volume, h is height, Δh is change in height, d is diameter, Δd is change in diameter, ϵ_a is axial strain, ϵ_v is volumetric strain, and A_f is the area of the actual failure plane.

Figure 1. The process used to validate internal cell photogrammetry and to obtain test parameters.



Key

S1: Analog specimen (38.1mm [1.5in.] diameter by 76.2mm [3.0in.] length, nominal) with targets used to derive location and orientation of internal cell cameras. Point cloud of targets was fixed (as obtained from DSLR camera). Camera locations/orientations were fixed (as obtained from the camera location/orientation step). S2: Larger analog specimen (44.5mm [1.75in.] diameter by 88.9mm [3.5in.] length, nominal) with targets used to calculate locations of targets on the specimen. *Nomenclature:* f is the focal length; $w:h$ are the format size dimensions (width to height ratio); $x:y$ are the principal point coordinates; and K_1, K_2, K_3, P_1, P_2 are lens distortion constants.

Figure 2. The process used to determine the volume of a specimen using internal cell cameras and the sensitivity of photograph interval on the volume of the specimen.

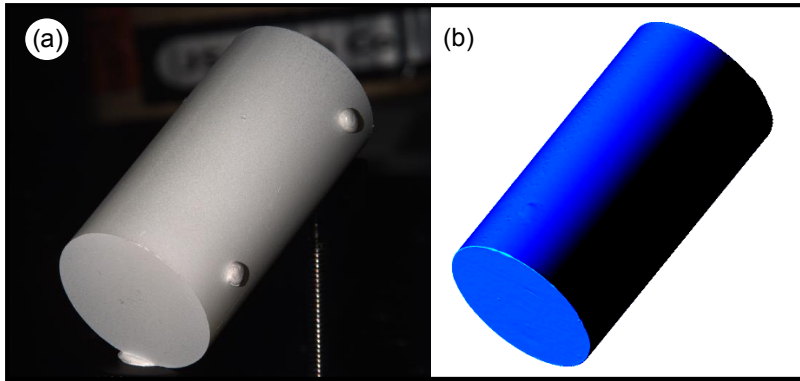
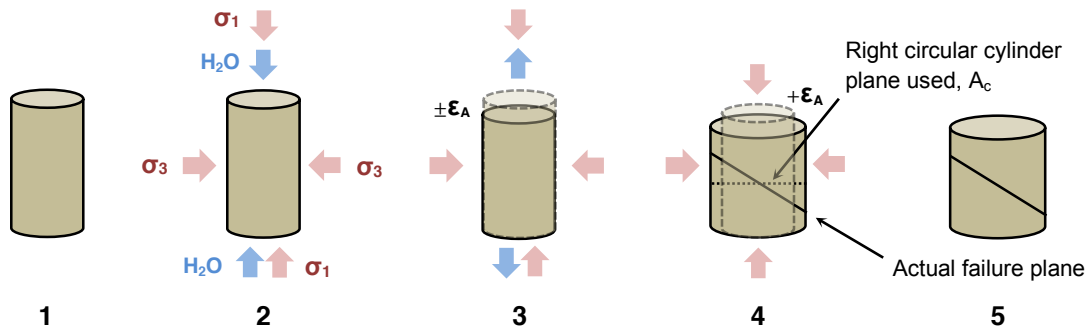


Figure 3. *a)* Photograph of, and *b)* three-dimensional, watertight model of small-acrylic analog specimen with spherical adhesive targets (removed during processing), as obtained during 3D scanning of specimen.

Expected Accuracy	Camera Resolution	Camera Calibration Method	Angles between Photos	Photo Orientation Quality	Photo Redundancy	Targets
Lowest Accuracy	Video 640x480	No calibration	Less than 15 degrees	Few targets per photo, low coverage	Points mostly on only two photos	No targets, all user marked
Average Accuracy	5-6 Megapixel	Inverse camera Calibrated camera	Between 15 and 60 degrees	15+ targets per photo, 25- 60% coverage	All points on 3+ photos	Some naturally lit targets Many good quality naturally lit
Highest Accuracy	11 Megapixel	Field calibrated camera	Between 60 and 90 degrees	35+ targets per photo, 50-80% coverage	Most targets on 8 or more photos	Retro-reflective

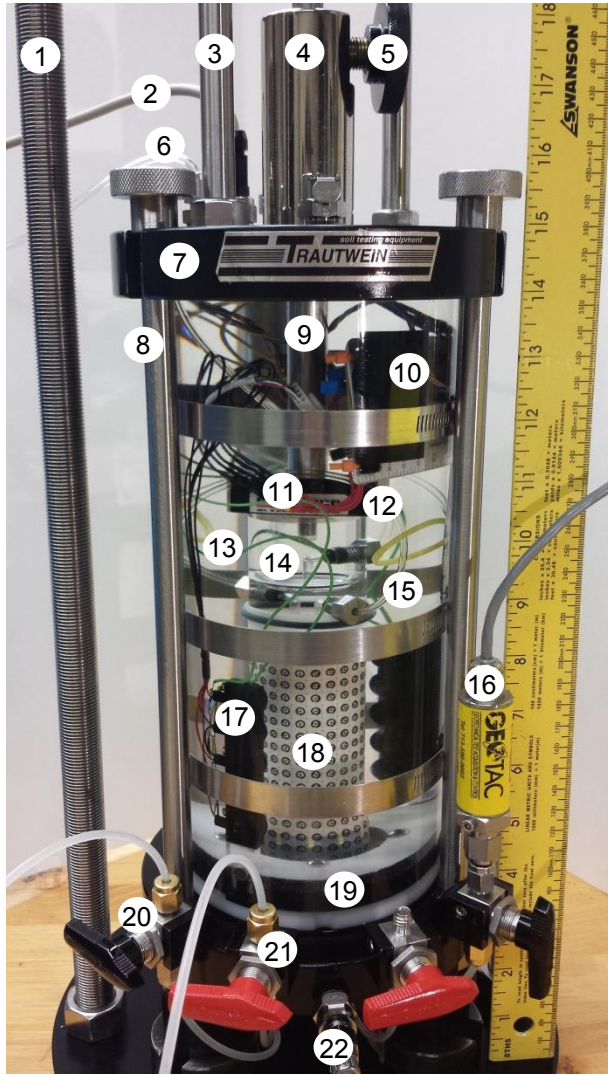
Shading highlights the characteristics of the photogrammetry methodology presented in this paper.

Figure 4. Factors affecting accuracy in photogrammetry (modified from Eos Systems, Inc. 2015).



1. *Pre-test:* Mass (m) and water content (w), measured; Volume (V) calculated using caliper measurements.
2. *Back-pressure saturation:* Drain lines filled. Total volume change (ΔV) from pore pump measurements. This volume change includes air 1) purged from lines, and 2) going into suspension.
3. *K_0 Consolidation:* Sample ΔV from pore pump measurements.
4. *Shearing:* m , w , and V assumed to be equal to post-test m , w , and V (if undrained); calculated from pore pump measurements (if drained).
5. *Post-test:* m and w , measured. Shear strength determined based on corrected area (A_c).

Figure 5. Typical measurements and calculations required for conventional triaxial compression test to determine phase diagram of soil specimen during test.



1. Load frame reaction rod (two quantity)
2. Cable with nine-pin feed-through connector (four pins for the internal load cell, two pins for the switchboard power supply, one pin for the video signal, two pins unused)
3. Uplift prevention rod (two quantity, for extension testing only)
4. Piston housing
5. Piston lock
6. Vacuum line for acrylic top cap vacuum connection
7. Top platen of cell
8. Fastening rod (three quantity)
9. Piston
10. Switchboard for camera timing (as shown in Salazar et al. [2015])
11. Electrical jumpers for individual camera power supply (red)
12. Internal load cell
13. Electrical jumpers for common grounding and video signals (green and yellow, respectively)
14. Acrylic top cap (triaxial extension vacuum cap shown)
15. Drain line (connection to top cap)
16. Pore pressure transducer
17. Camera tower (two quantity, 5 cameras each)
18. Soil specimen within membrane (RAD-coded targets adhered to membrane)
19. Rotating Delrin[®] bearing track
20. Top drain line and drain valve (black)
21. Bottom drain line and drain valve (red)
22. Cell pressure application line

Figure 6. Photograph of the kaolinite specimen within the photogrammetrically instrumented triaxial cell during the shearing stage of the extension test.

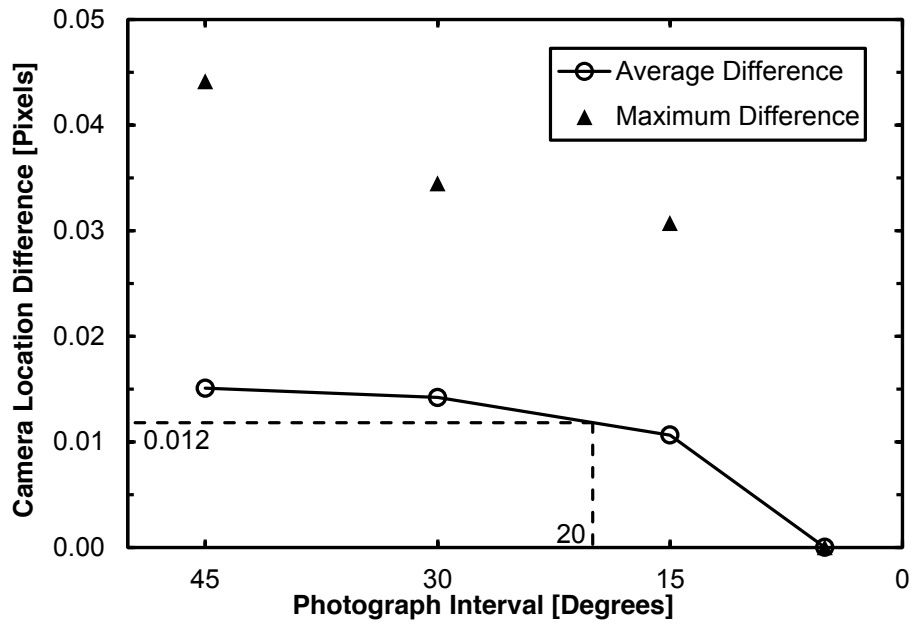


Figure 7. Derived camera location difference as a function of photograph interval.

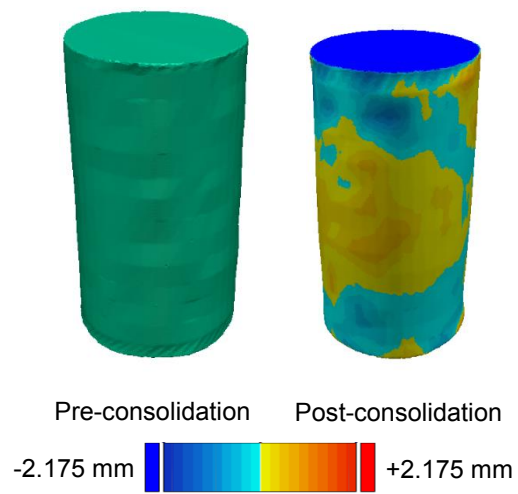
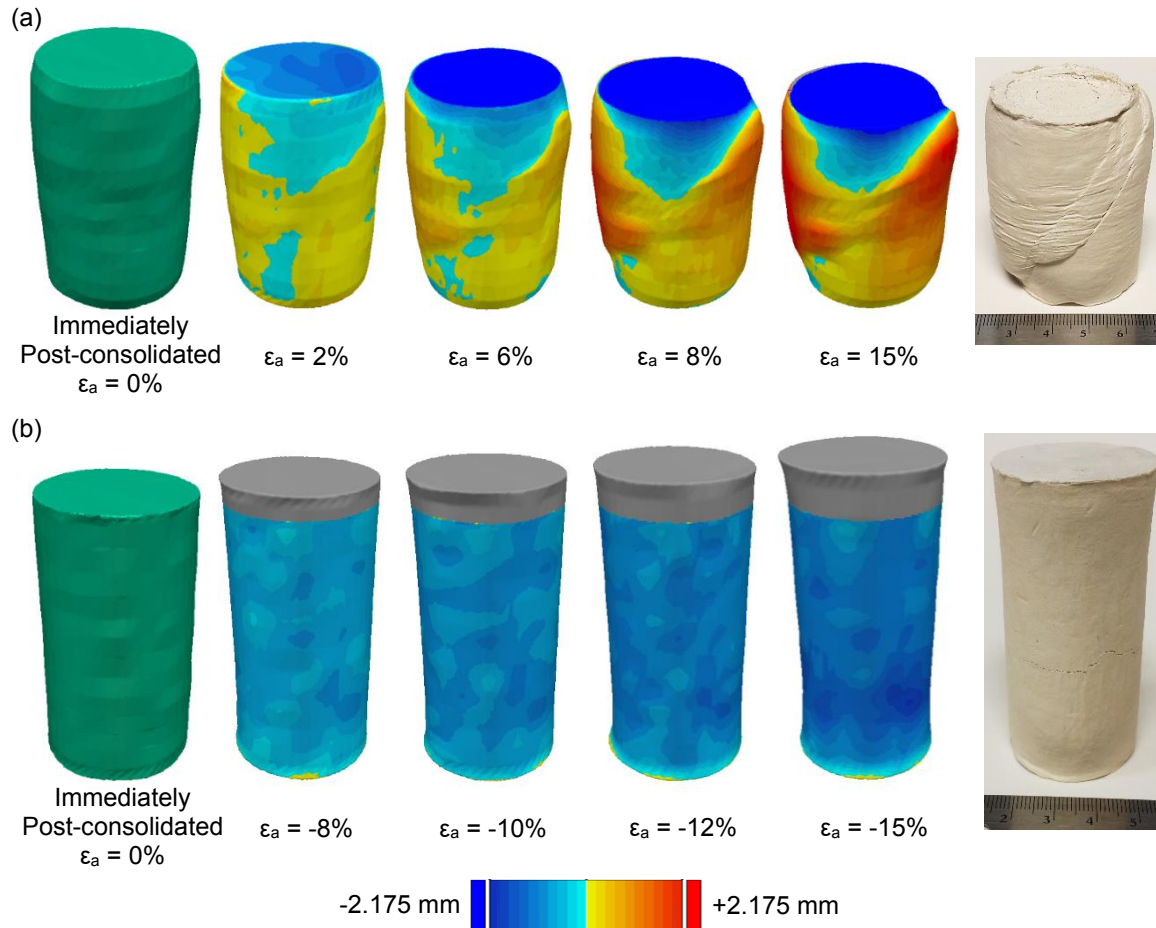


Figure 8. Strain visualization of photogrammetry-obtained, three-dimensional models of kaolinite specimen during K_0 -consolidation phase of triaxial test (warm colors indicate positive deformation and cool colors indicate negative deformation).



Note: Photographs on the right are of post-test, oven-dried specimens.

Figure 9. Strain visualization of photogrammetry-obtained, three-dimensional models of kaolinite test specimen during *a*) conventional triaxial compression, and *b*) reduced triaxial extension tests up to 15 percent axial strain during shearing (warm colors indicate positive deformation and cool colors indicate negative deformation).